Accepted Manuscript

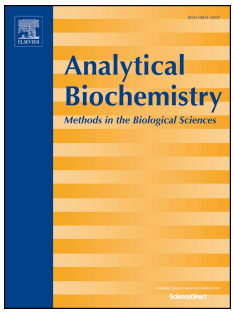

A novel electrochemical immunosensor based on ITO modified by carboxyl-ended silane agent for ultrasensitive detection of MAGE-1 in human serum

Aslı Gündoğdu, Elif Burcu Aydın, Mustafa Kemal Sezgintürk

PII: S0003-2697(17)30360-3

DOI: 10.1016/j.ab.2017.08.018

Reference: YABIO 12778

To appear in: *Analytical Biochemistry*

Received Date: 12 July 2017

Revised Date: 25 August 2017

Accepted Date: 26 August 2017

Please cite this article as: Aslı. Gündoğdu, E.B. Aydın, M.K. Sezgintürk, A novel electrochemical immunosensor based on ITO modified by carboxyl-ended silane agent for ultrasensitive detection of MAGE-1 in human serum, *Analytical Biochemistry* (2017), doi: 10.1016/j.ab.2017.08.018.

A novel electrochemical immunosensor based on ITO modified by carboxyl-ended silane agent for ultrasensitive detection of MAGE-1 in human serum

Aslı Gündoğdu[a], Elif Burcu Aydın[b*], Mustafa Kemal Sezgintürk[c]

[a]Namık Kemal University, Faculty of Science, Chemistry Department, Biochemistry Division, Tekirdağ, TURKEY

[b]Namık Kemal University, Scientific and Technological Research Center, Tekirdağ-TURKEY

[c]Çanakkale Onsekiz Mart University, Faculty of Engineering, Bioengineering Department, Çanakkale-TURKEY

***Corresponding Author:**

e-mail: b_e_bahadir@hotmail.com

ebbahadir@nku.edu.tr

Tel:+90 282 250 11 37

Abstract

A new, low-cost electrochemical immunosensor was developed for rapid detection of Melanoma-associated antigen 1 (MAGE-1), a cancer biomarker. The fabrication procedure of immunosensor was based on the covalent immobilization of anti-MAGE-1, biorecognition molecule, on ITO electrode by carboxyethylsilanetriol (CTES) monolayer. The biosensing MAGE-1 antigen was monitored by using electrochemical impedance spectroscopy (EIS) and cyclic voltammetry (CV) technique. Apart from these techniques, single frequency impedance (SFI) was used for investigation of antibody-antigen interactions. Scanning electron microscopy (SEM), fourier transform infrared spectroscopy (FTIR), atomic force microscopy (AFM) were utilized for characterization of the proposed biosensor. To fabricate highly sensitive, good stability immunosensor, some parameters were optimized. Under optimal conditions, the developed electrochemical immunosensor for MAGE-1 exhibited a dynamic range of 4 fg/mL and 200 fg/mL with a low detection limit of 1.30 fg/mL. It had acceptable repeatability (5.05%, n=20) and good storage stability (3.58% loss after 10 weeks). Moreover, this electrochemical immunosensor has been successfully applied to the determination of MAGE-1 in human serum samples.

Keywords: Melanoma-associated antigen 1, electrochemical immunosensor, indium tin oxide, carboxyethylsilanetriol

1. Introduction

Melanoma-associated antigen (MAGE) was firstly reported in melanoma cases as a tumour-associated antigen [1]. Today it is confirmed that melanoma-associated antigen proteins constitutes a super-family which comprises more than 60 genes in human. MAGE-I and MAGE-II proteins are the subdivided members of this super family [2, 3]. Not only MAGE-I proteins are generally associated with testis cancer antigens, but also it has been reported that some MAGE I proteins have important functions in particular somatic tissues [4, 5]. Moreover, as recently reported that during the embryonic development in spinal cord and brain stem cells, certain MAGE-A members are also expressed [6]. From a cancer perspective, in certain cancer types such as breast, ovary, lung, and bladder, it is surely known that MAGE-I proteins are highly synthesized [7, 8]. Further, some experiments showed that in malignant cancers, MAGE-I has also been expressed. Additionally, determination of MAGE in cancer patients can also be attributed to a poor prognosis which supports the idea of contribution of MAGE proteins to malignancy [3].

Electrochemical immunosensors have gained considerable attention owing to their benefits such as simple operation, fast and cost-efficient detection and high sensitivity [9]. Due to the advantages of convenience, low-cost, fast response, easy operation and high sensitivity, they have been usually utilized in several analytical fields [10]. Electrochemical impedimetric immunosensors open the door to a large number of different applications based on a platform such as solid electrodes (gold, carbon electrodes) and transparent conductive oxides (indium tin oxide (ITO), fluorine doped oxide (FTO)). The application of ITO electrodes as working electrode has gained considerable interest owing to their unique characteristics such as good optical transparency, high electrical conductivity, wide electrochemical working range, excellent substrate adhesion, and stable electrochemical/physical features [11-13]. A lot of studies have been carried out to develop ITO based electrochemical and optic sensors and biosensors. The immobilization of biorecognition molecules such as antibodies, enzymes or DNA probes has been immobilized to ITO electrode via a self-assembled monolayer of different silane chemicals such as TESU [14], (3-isocyanatopropyl) triethoxysilane (IPTES) [15], 3-aminopropyltriethoxy silane (APTES) [16-20], (3-glycidoxypropyl) dimethoxysilane [21], (3-glycidoxypropyl) dimethoxysilane [10], N-(2-aminoethyl)-3-aminopropyltrimethoxysilane [22], 3-mercaptopropyl trimethoxysilane (3-MPTMS) [23], 3-aminopropyltrimethoxy silane (APTMS) [24]. Apart from this technique, ITO electrodes are prepared to immobilization of biorecognition element by using electrochemical deposition [25, 26], Electrophoretic deposition [27, 28], adsorption techniques [28-30].

The developed biosensors for MAGE-1detection are very scarce and there are commercial ELISA kits for MAGE-1 detection. Biosensors represent a potential alternative to ELISAs, and provide probably

one of the most promising ways to solve problems concerning simple, fast, reproducible, and cheap detection [31]. The cost of such ITO based immunosensor is approximately 0.5 € and the preparation step of such immunosensor is easy. But the cost of ELISA kit is approximately 500 €. Furthermore, ELISA analysis has several steps and requires a lot of time. A well of ELISA can only be used once and it is not suitable for regeneration. ITO based such immunosensor is reusable and it reduces analysis cost.

Herein, for the first time, an impedimetric immunosensor was constructed based on silane based ITO electrode with carboxyl end groups for detection of MAGE-1 sensitively. To construct our immunosensor, carboxyethylsilanetriol (CTES) was used as a silane etriol molecule, anti-MAGE-1 antibody was used as recognition biomolecule and ITO was used as a working electrode. Anti-MAGE-1 antibody was immobilized covalently on the ITO electrode surface through self-assembled monolayer of CTES [32]. Characterization of this silanetriol monolayer on ITO surfaces and the anti-MAGE-1 antibody layer on the ITO electrode surface were performed EIS, cyclic voltammetry (CV), fourier transform infrared spectroscopy (FTIR). Microscopic techniques such as SEM and AFM were utilized for imaging the electrode surface alterations. The characterization of the electrode interfaces is significant and provides good information about the surface features of the immunosensor that has crucial importance to obtain a sensitive and reproducible biosensor. Furthermore, the specific recognition of MAGE antigens by immobilized anti-MAGE-1 antibodies was characterized by single frequency impedance (SFI). SFI technique gives information about the interactions of antibody-antigen systems [33]. By using EIS technique, the detection range, detection and quantification limits, repeatability, reproducibility, stability and practical applicability studies were performed. Consequently, the measurements exhibited that our biosensor had sensitive, selective and stabile results.

2. Experimental

2.1. Reagents and Materials

All chemicals used were of analytical grade and obtained from Sigma-Aldrich (St. Louis, MO, USA). ITO-coated polyethylene terephthalate (PET) films (surface resistivity:60 Ω^2, transmittance at 550 nm: >79%) were purchased from Sigma Aldrich. Ultra-pure water was used for preparation of phosphate buffer and electrolyte solution. Anti-MAGE-1 antibody, MAGE-1 antigen and bovine serum albumin (BSA) (0.5%) were prepared by using phosphate buffer (PBS; 50 mM, pH 7.0) were stored at -20 ^{o}C. A silane etriol compound, carboxyethylsilanetriol (CTES), 1-ethyl-3-(3-dimethyl aminopropyl)carbodiimide hydrochloride (EDC) and N-hydroxysuccinimide (NHS) were purchased from Sigma-Aldrich. 5 mM $K_4[Fe(CN)_6]$, $K_3[Fe(CN)_6]$ in phosphate buffer was used as redox probe.

2.2. Apparatus

Electrochemical experiments such as CV, EIS, and SFI were performed on a Gamry Potentiostat/Galvanostat (Reference 1000, Gamry Instruments, Warminster, PA, USA) with a conventional three electrode system. The experimental parameters for CV: scan rate 100mVs^{-1} and step size 10 mV. The experimental parameters for EIS: initial frequency 50000 Hz, final frenquency 0.05 Hz and point 5. The ITO thin film (2*20 mm) was employed as a working electrode while platinum wire and Ag/AgCl (3M KCl) served as counter and reference electrode, respectively. The reference electrode and counter electrode were produced from BASi (West Lafayette, IN, USA). The characterization of the modified ITO thin films was performed by SEM (FEI-Quanta FEG 250 Model), AFM (NanoMagnetic Instruments, AFM PLUS+). SEM and AFM analyses were carried out at 5kV acceleration and with tapping mode. FTIR measurements were performed by using Bruker, Vertex 70 ATR (Germany) FTIR equipped with diamond. FTIR spectra in the range 4000–400 cm^{-1} were recorded in order to investigate the nature of the chemical bonds formed. The SEM, AFM and FTIR measurements were performed at the Scientific and Technological Research Center of NKU (NABILTEM).

2.3. Preparation of Working Electrode

ITO slices were cleaned with successively by sonication in acetone, soap solution and ultra-pure water for 10 min, and then rinsed with ultra-pure water. The cleaned ITO was then dipped into a solution of 1:1:5 (v/v) H_2O_2 (30%)/ NH_4OH (30%)/ H_2O for 90 min. Finally, they were washed with ultra-pure water. Before the silanization, the ITO slices were dried by using argon gas.

2.4. Fabrication procedure of MAGE-1 biosensor

The hydroxylated ITO electrodes were dipped into a 0.5% solution of CTES in ultra-pure water over night at room temperature. After incubation, the ITO slices were washed with ultra-pure water to remove the physically absorbed silanes from the ITO electrode surface [10, 14]. The modified ITO slices were then dried by using argon gas. Thus, carboxyl groups were formed on ITO electrode. These carboxyl groups formed on ITO electrodes were activated by NHS/EDC chemistry [32]. The anti-MAGE-1 antibodies were immobilized onto the prepared ITO electrode through the linkage between amino groups of antibodies and the active carboxyl groups of CTES SAMs. After incubation, the electrodes were washed with ultra-pure water to remove physically absorbed antibodies. Subsequently, BSA (0.5%) was used to prevent the non-specific interactions that can be formed in detection MAGE-1 step on the modified ITO electrode. The biosensor fabrication strategy is shown in Scheme 1.

3. Results and Discussion

3.1. Design Strategy of the impedimetric MAGE-1 immunosensor

The construction procedure of impedimetric MAGE-1 biosensing electrodes is illustrated in Scheme 1. The first step of fabrication procedure was cleaning of ITO slices. This cleaning is significant as organic contaminants on ITO surface could affect the response. Before the construction a silane layer on ITO electrode, it was hydroxylated. Then, the activated ITO surface was coupled with CTES including carboxyl groups on its ends. These carboxyl groups were activated by using NHS as coupling agent, EDC as activator [34]. The biorecognition elements, anti-MAGE-1 antibodies, were immobilized onto CTES modified ITO electrode through the amide bonds between amino groups of antibody and active carboxyl groups of CTES [35]. Then, BSA was blocked the non-specific binding sites [36]. Finally, the CTES modified MAGE-1 biosensor was fabricated successfully. Thus, this fabricated biosensor was ready for MAGE detection. The construction process of biosensing interface was monitored by EIS and CV measurements. 5 mM hexacyanoferrate (II) (ferrocyanide) and 5 mM hexacyanoferrate (III) (ferricyanide) were used as redox probe.

Immobilization Scheme 1. Schematic diagram of the fabrication of the impedimetric MAGE-1 biosensor and the detection of MAGE-1 antigen

FTIR spectra of CTES modified ITO surface and immobilization of anti-MAGE-1, BSA and MAGE-1 on the ITO electrode surface are shown in Figure 1. As shown in figure 1A, the strong peak observed at around 1650 cm^{-1} is characteristic of the stretching mode νC=O of the carbonyl involved in carboxylic acid groups on CTES. The broad band between 3200 and 3600 cm^{-1} corresponded to the νOH vibration and another band assigned to νC−O−H in plane mode were observed at 1422 cm^{-1} [22, 37]. Figure 1B shows the FTIR spectrum of the same surface after anti-MAGE-1 immobilization on ITO electrode. The observation of broad and intense bands for amide I at ~1655 cm^{-1} and for amide II at ~1525 cm^{-1} clearly indicates the presence of the amide bonds between anti-MAGE-1 and carboxyl groups of CTES [38]. Figure 1C illustrates the FTIR spectrum of the same surface after interaction between anti-MAGE-1 and MAGE antigen on ITO electrode. The increment in peak areas at ~1655 cm^{-1} and ~1525 cm^{-1} provided that the increase in amino and carboxyl groups.

Figure 1. FTIR spectra of the fabrication steps of the impedimetric MAGE-1 biosensor

EIS, as an efficient technique to monitor the interfacial features of modified ITO slices, was utilized to follow the construction process of the ITO electrode. Figure 2A shows the impedance spectra (Nyquist plots) of stepwise construction procedure. EIS represents the response of an electrochemical system as a function of the frequency including an impedance spectra known as Nyquist plot which can be modelled with the Randles equivalent circuit. The circuit displays a semicircle at higher frequencies belongs to the parallel double layer capacitance (C_{dl}) and charge-transfer resistance (R_{ct}). The R_{ct} value of this system is equal to the diameter of the semicircle. At lower frequencies, a straight line belongs to the Warburg diffusion impedance (Z_w). The value of R_{ct} depends on the dielectric and insulating properties at the electrode/electrolyte interface. So, the diameter (R_{ct}) can be utilized to identify the

interface features of the electrode. In sum, R_{ct} derived from the diameter of semicircles. Generally, the contribution of diffusion to the overall impedance is smaller than large R_{ct} value. Because chemical species is adsorbed at the electrode-solution interface, the R_{ct} value changes [39, 40].

Figure 2. Nyquist plots and cyclic voltammograms of MAGE-1 biosensor (-▼-▼-: hydroxylated ITO electrode, -♦-♦-: ITO/CTES, -●-●-: ITO/CTES/EDC-NHS, -▲-▲-: ITO/CTES/EDC-NHS/anti-MAGE-1, -■-■-: ITO/CTES/EDC-NHS/anti-MAGE-1/BSA)

Throughout the formation procedure of silane etriol monolayer, immobilization of the antibody, binding of antigen were monitored by using EIS technique via the variation in electron transfer resistance. As shown in Figure 2A, impedance values differed in each step of surface modification during the fabrication process. The hydroxylated ITO had a small R_{ct}, indicating a small electron transfer resistance. After silanization process with CTES, the R_{ct} value increased. It could be attributed to the difficult electronic transport at electrode surface interface due to SAM formation. After activation of carboxyl groups via NHS/EDC chemistry R_{ct} values increased. The formation of active carboxyl groups obstructs the diffusion of redox probe, therefore the R_{ct} value increased. When the electrode was conjugated with anti-MAGE-1 antibody, the R_{ct} increased, this indicated that the successful immobilization of anti-MAGE-1 antibody on ITO electrode surface. So, an additional barrier was formed and it blocked the electron transfer between the redox probe and the ITO electrode. Similarly, an increment in the R_{ct} was seen after BSA immobilization on the ITO electrode, owing to that BSA prevents the electron transfer on the electrode surface. These obtained results suggested the successful fabrication of the biosensor.

CV is a useful technique to characterize electrodes [41]. As shown in figure 2B, the differences in peak current of the $Fe(CN)_6^{-3/-4}$ redox couple showed the alteration at each step of the surface modification of ITO electrode. The hydroxylated ITO had a reversible electrochemical response. The modification of ITO surface with CTES presented a decrease in peak current. This result is attributed to that non-active carboxyl group causes difficult electron transfer reaction on the electrode surface. After activation of carboxyl groups, peak currents decreased due to a repulsive interaction between active carboxyl groups and anionic redox couple. Anti-MAGE antibody, which was modified on the ITO/CTES/NHS/EDC electrode through the amide bonding interaction between active carboxyl group and amino groups of anti-MAGE, caused the blockage of the ITO electrode surface for oxidation/reduction of the redox couple. After blocking active sides of electrodes with BSA, peak currents values decreased owing to insulating character of BSA protein. In detection step, interaction between anti-MAGE antibody and MAGE antigen increased diffusion barrier and decreased the peak current values.

3.2. Surface Characterization of Modified Electrodes by SEM and AFM

The surface morphology of ITO slices was clarified by using SEM (Figure 3) and AFM (Figure 4). The alteration of electrode surface and formed functional layer can be monitored by using SEM and AFM. In SEM measurements, after hydroxylation step, ITO had uniform surface (Fig 3A). Fig 3B shows that the surface morphology of CTES modified electrode is clearly different from that of hydroxylated ITO electrode. Furthermore, the CTES film on the ITO electrode was dense and homogenous with a few globular aggregates. The formation of CTES monolayer displayed that the electrode surface was changed. The SEM image of ITO/CTES/NHS/EDC electrode displays smooth surface (Fig. 3C). After immobilization of anti-MAGE antibody on ITO/CTES/NHS/EDC electrode, a well coverage of the anti-MAGE antibodies on the electrode are seen in Fig 3D. After BSA blockage, island-like morphology was seen on ITO electrodes (Fig. 3E). The interaction between MAGE and anti-MAGE, is shown in Fig. 3F. All the SEM images demonstrate that the covalent coupling of CTES onto the ITO electrode was performed successfully and it is suitable material for immobilization of antibody on ITO surface.

Figure 3. SEM images of proposed ITO immunosensor

AFM images were recorded to monitor the morphological differences of the electrode surface obtained after each modification step. Hydroxylated ITO includes grains with an area roughness of 3.69 nm and a root mean squre (rms) roughness of 4.56 nm on a 5 x 5 µm scale. The AFM images illustrated that the hydroxylated ITO (Fig. 4A) had a uniform and homogenous surface. However, the ITO/CTES electrode showed that the CTES molecule was distributed homogenously and the roughness height increased (Fig. 4B). CTES modified ITO electrode includes grains with an area roughness of 5.43 nm and an rms roughness of 6.85 nm on a 5 x 5 µm scale. This arrangement provides the CTES SAMs with carboxyl groups to serve as a template for chemical anchoring of protein or several molecule layer. Figure 4C demonstrates the surface morphology of anti-MAGE-1 α antibody immobilized onto the surface of CTES modified ITO. As seen in figure 4C, anti-MAGE-1 antibody had globular structure due to its protein nature. The image provided that the CTES modified ITO could succeed in serving as a template for immobilization of anti-MAGE-1 antibody. This is important for the sensitivity and the reproducibility of biosensor. Anti-MAGE-1 α modified ITO electrode includes grains with an area roughness of 71.18 nm and an rms roughness of 98.32 nm on a 5 x 5 µm scale. After blocking reactive carboxyl ends of CTES with BSA, the electrode surface transformed into a heterogeneous globular-like structure, with an increase in thickness. Thus, a highly uniform immunoelectrode surface was constructed (Figure 4D). BSA modified ITO electrode includes grains with an area roughness of 4.06 nm and an rms roughness of 17.00 nm on a 5 x 5 µm scale. As seen figure 4E, the interaction between anti-MAGE-1 and and MAGE-1 caused an increase in roughness height and an increase in thickness, that indicate successful interaction between and antigen. Also, after the interaction, modified ITO electrode includes grains with an area roughness of 70.29 nm and an rms roughness of 92.31 nm on a 5 x 5 µm scale.

Figure 4. AFM images of immobilization steps of developed immunosensor

3.3 Optimization experiments of biosensor

Optimization stages are significant and necessary for fabrication of sensitive, stable, repeatable and reproducible biosensor. Therefore, the utilized amount of CTES, antibody concentration, antibody incubation time and antigen incubation time were optimized.

The modification of ITO electrode with CTES is a significant step for immobilization of anti-MAGE antibodies onto ITO electrode surface. For this reason, three different CTES concentrations (0.25%, 0.5% and 0.75%) were tried. The signal of 0.25% and 0.75% CTES concentrations were similar. Because of this, the signal 0.5% concentration was higher than these of two concentrations and 0.5% concentration was chosen as the optimal. The calibration graphs belonging to CTES concentration optimization steps are illustrated in Figure SI-1.

The next optimization stage was anti-MAGE antibody concentration required to form biosensing layer. To fabricate a sensitive biosensor, this stage was very important. Because of this, 3 different concentrations (5.5 ng/mL, 11 ng/mL, 33 ng/mL) were used. An increment in antibody concentration caused a bit increase in signal. However, the signals obtained from these concentrations were similar. Therefore, 5.5 ng/mL anti-MAGE concentration was chosen as optimum amount. The calibration graphs belonging to antibody concentration optimization steps are illustrated in Figure SI-2. Other optimization step was incubation period of CTES modified ITO in PBS solution containing anti-MAGE antibody. This stage is important because this step effects the binding efficiency of antibody. The studied incubation times are 30 min, 45 min and 60 min. Both of three incubation periods had a similar signal, because of this 30 min was chosen as optimum (Figure SI-3). The concentrations of MAGE antibody and incubation period of anti-MAGE-1 antibody were optimized successfully.

The last optimization parameter was the antigen (MAGE-1) incubation time. Therefore, the fabricated immunoelectrodes were immersed PBS solution containing MAGE-1 in different times (30, 45, 60, 75 min). The short incubation period (30 min) was insufficient to bind MAGE-1 antigens to their antibodies. At high MAGE-1 antigen concentrations, the longer incubation periods (60 and 75 min) caused a decrease in signal (Figure SI-4), that could be orginated from a surface damage on the modified ITO electrode. Consequently, 45 min was chosen as the incubation period for MAGE-1 protein (Figure SI-4).

3.4. Analytical studies of the biosensor

Under the optimized experimental conditions, calibration plot, repeatability, reproducibility experiments were studied.

Firstly, linear range of MAGE biosensor was determined. The calibration curve of MAGE biosensor was constructed by using impedimetric responses, electron transfer resistance, which was estimated by the equation:

$\Delta R_{ct} = R_{ct}(\text{MAGE-1}) - R_{ct}(\text{BSA})$

Where R_{ct}(MAGE-1) is the value of the electron transfer resistance after MAGE-1 was coupled onto ITO electrode, R_{ct}(BSA) is the value of electron transfer resistance after BSA blocking the free active carboxyl groups on the ITO electrode.

Figure 5. (A) Nyquist plots and (C) cyclic voltammograms of MAGE-1 biosensor with different concentrations of MAGE-1 antigens, (B) calibration curve of MAGE-1 biosensor

Fig. 5 represents the CV voltammograms and Nyquist plots belong to the immunosensors after incubation in increasing concentrations of the MAGE-1 antigen. The changes of the ΔR_{ct} was utilized as a response of the interaction between the anti-MAGE-1 antibody and MAGE-1 antigen. The diameter of Nyquist circle increased with increment MAGE-1 antigen levels (Fig. 5A). The reason of this increment was the binding of more antigens to immobilized antibodies. The ΔR_{ct} was drawn versus the MAGE-1 antigen concentration to attain a calibration plot (Fig. 5B). The range of sensitivity was monitored between 4 fg/mL and 200 fg/mL and limit of detection ($3*S_{blank}/m$) was 1.30 fg/mL and limit of quantification ($10*Sb_{lank}/m$) was 3.90 fg/mL with a coefficient of 0.98%. In this equation, S_{blank} is the signal of blank sample and m is the slope [42]. In contrast to the impedance curve there is a decrease at peak currents in CV voltammograms during the increment of MAGE-1 concentrations (Fig 5C). An increase of the MAGE-1 concentration formed an insulator protein layer on ITO surface, thus the peak currents were decreased. Consequently, a gradual increase in MAGE-1 concentration caused a gradual increase in R_{ct} (semicircle diameter) and a decrease in peak values.

To investigate the analytical performance, another method, square wave voltammetry (SWV) was performed to support CV and EIS results. The low concentration of MAGE-1 concentration had a high peak. An increase in MAGE-1 concentration caused a decrease in peak currents. Also, the variation between BSA and MAGE-1 concentration peak increased. This leads to a linear increase in MAGE-1 protein binds to the surface. The obtained calibration curve is illustrated in Figure SI-5.

In this study, SFI was applied to monitor the interactions between antigen-antibody systems [33]. Few studies can be found in the literature for this purpose. The principle of this technique is based on the variations on the surface and kinetic parameters during the interaction at a fixed frequency. These variations are recorded in impedance values versus time at a fixed frequency [43]. In this study, working frequency was chosen as 45 Hz by using Bode Plot. The total measurement time was 30 min, which was optimum binding period. The green curve illustrates the change of impedance as a function

of time. The pink curve illustrates the phase angle and charge transfer results from the interaction between the MAGE-1 antigen-anti-MAGE-1 antibody (Figure 6).

Figure 6. SFI spectra obtained from anti-MAGE-1 antibody and MAGE-1 antigen interaction

Kramer's Kronig transform is used to monitor whether the biosensors are affected from the external factors. The principle of this method is based on estimation of reel part of impedance data by using imaginative part or calculation of imaginative part by using reel part [32, 44, 45]. The goodness of fit values for different biosensor surface are illustrated in Table 1. The plots of the Kramers–Kronig Transforms are displayed in Figure SI-6.

Repeatability, reproducibility and stability are three important parameters for evaluation of immunosensor fabricated for analytical purposes. The repeatability of the immunosensor was analyzed at MAGE-1 concentration of 80 fg/mL with 20 different ITO electrodes, which were prepared in same conditions. By these repeatability examinations, the correlation coefficient, average value and standard deviation 5.54%, 80.6 fg/mL and 4.467 fg/mL, respectively. The reproducibility of the fabricated MAGE-1 biosensor was investigated by constructing different immunosensors (10 MAGE-1 calibration curves were drawn by using 80 disposable electrode) to detect MAGE-1 independently. All of these biosensors displayed the same linearity in the range between 4-200 fg/mL for MAGE-1. The relative standard deviations were also calculated by using the slopes of the linear equations attained from these immunosensors as 5.05%. These results showed that the MAGE-1 immunosensor have an acceptable fabrication reproducibility in MAGE-1 detection. The stability of the developed biosensor was analyzed by measuring its impedance response to MAGE-1 each week. After 10 weeks only 3.58% loss was seen on the impedance signal (at 80 fg/mL), proving the excellent stability of the immunosensor (Figure SI-7).

The regeneration ability of the electrochemical immunosensor is important for the sensor applications. To test reusability of biosensor, the linkage between anti-MAGE-1 antibody and MAGE-1 antigen was broken under acidic conditions (0.1% HCl in ultra-pure water). In brief, the biosensor was regenerated after incubating the used electrode in the solution of 0.1% in HCl in ultra-pure water for 5 min to remove MAGE-1 antigen from the anti-MAGE-1 antibody, as acid broke this affinity interaction. After four regeneration step, biosensor had 93% of its initial activity. At the end of fifty regeneration step, biosensor got damaged (Figure SI-8). This obtained result is important because the reusability decreases the cost of biosensor.

For a biosensor, one of the most significant analytical parameters is the selectivity towards the target analyte. To test selectivity of the proposed biosensor, interface materials such as different biomarkers (Sex-determining region Y-box 2 (SOX2), Receptor for Activated C Kinase (RACK1), Tumor necrosis factor α (TNF α)) and drugs (ampicillin, ciprofloxacin, amoxicillin) were added PBS solution containing MAGE-1 antigen and without MAGE-1 antigen. As seen figure SI-9, the interface

materials did not affect the biosensor signal. Furthermore, five human serum samples (supplied by Namık Kemal University Faculty of Medicine) were analysed to prove the practicality and selectivity of the biosensor. The obtained results are given in Table1. Apart from our biosensor these five different human serum samples were examined by using enzyme linked immunosorbent assay (ELISA) method. The detection range of this ELISA kit was in the range of 0.625-40 ng/mL. The results were attained by using the new developed immunosensor was in agreement with that of the ELISA results, that indicates our immunosensor can be apply to serum samples.

4. Conclusion

In conclusion, we reported a novel MAGE-1 electrochemical immunosensor based on ITO electrode. The principle of this immunosensor was based on sensing the interaction between anti-MAGE-1 antibody and MAGE-1 antigen by electrochemical impedance spectroscopy. This study illustrated that CTES modified ITO had carboxyl end groups for the immobilization of antibody molecules. And antibody molecules including amino groups bound carboxyl groups of CTES via amide bond. This well designed immunosensor displayed a low detection limit of 1.30 fg/mL as well as wide linear range from 4 to 200 fg/mL for MAGE-1 detection. Besides, the proposed immunosensor showed excellent analytical performance for the measurement of MAGE-1 in human serum samples. The practical utility of the developed immunosensor was proved by spiking known concentrations of MAGE-1 antigen in the human serum samples. This developed MAGE-1 biosensor has the promise for potential applications in clinical diagnosis. Our immunosensor displays high specificity, sensitivity, good reproducibility and long stability.

Acknowledgment

The financial support from TÜBİTAK (The Scientific and Technological Research Council of Turkey, Project number: 113 Z 678) is gratefully acknowledged.

5. References

[1] P. van der Bruggen, C. Traversari, A gene encoding an antigen recognized by cytolytic T lymphocytes on a human melanoma, Science, 254 (1991) 1643.
[2] P. Chomez, O. De Backer, M. Bertrand, E. De Plaen, T. Boon, S. Lucas, An overview of the MAGE gene family with the identification of all human members of the family, Cancer research, 61 (2001) 5544-5551.
[3] A.J. Simpson, O.L. Caballero, A. Jungbluth, Y.-T. Chen, L.J. Old, Cancer/testis antigens, gametogenesis and cancer, Nature Reviews Cancer, 5 (2005) 615-625.
[4] W. Liu, S. Cheng, S.L. Asa, S. Ezzat, The melanoma-associated antigen A3 mediates fibronectin-controlled cancer progression and metastasis, Cancer research, 68 (2008) 8104-8112.
[5] E.M. Wilson, Androgen receptor molecular biology and potential targets in prostate cancer, Therapeutic advances in urology, (2010).
[6] M.F. Gjerstorff, L. Harkness, M. Kassem, U. Frandsen, O. Nielsen, M. Lutterodt, K. Møllgård, H.J. Ditzel, Distinct GAGE and MAGE-A expression during early human development indicate specific roles in lineage differentiation, Human reproduction, 23 (2008) 2194-2201.

[7] M. Sang, L. Wang, C. Ding, X. Zhou, B. Wang, L. Wang, Y. Lian, B. Shan, Melanoma-associated antigen genes–an update, Cancer letters, 302 (2011) 85-90.
[8] M.J. Scanlan, A.O. Gure, A.A. Jungbluth, L.J. Old, Y.-T. Chen, Cancer/testis antigens: an expanding family of targets for cancer immunotherapy, Immunological reviews, 188 (2002) 22-32.
[9] W. Liu, H. Yang, S. Ge, L. Shen, J. Yu, M. Yan, J. Huang, Application of bimetallic PtPd alloy decorated graphene in peroxydisulfate electrochemiluminescence aptasensor based on Ag dendrites decorated indium tin oxide device, Sensors and Actuators B: Chemical, 209 (2015) 32-39.
[10] L. Yang, Y. Li, AFM and impedance spectroscopy characterization of the immobilization of antibodies on indium–tin oxide electrode through self-assembled monolayer of epoxysilane and their capture of Escherichia coli O157: H7, Biosensors and Bioelectronics, 20 (2005) 1407-1416.
[11] H. Zeng, D.A.Y. Agyapong, C. Li, R. Zhao, H. Yang, C. Wu, Y. Jiang, Y. Liu, A carcinoembryonic antigen optoelectronic immunosensor based on thiol-derivative-nanogold labeled anti-CEA antibody nanomaterial and gold modified ITO, Sensors and Actuators B: Chemical, 221 (2015) 22-27.
[12] M.Z.H. Khan, Effect of ITO surface properties on SAM modification: A review toward biosensor application, Cogent Engineering, 3 (2016) 1170097.
[13] J. Lin, W. Qu, S. Zhang, Electrochemical immunosensor for carcinoembryonic antigen based on antigen immobilization in gold nanoparticles modified chitosan membrane, Analytical sciences, 23 (2007) 1059-1063.
[14] E. Bahadır, M. Sezgintürk, Label-free, ITO-based immunosensor for the detection of a cancer biomarker: Receptor for Activated C Kinase 1, Analyst, 141 (2016) 5618-5626.
[15] M. Ozmen, K. Can, M. Ersoz, Immobilization of albumin on indium-tin oxide (ITO) surface via isocyanate linkage, Journal of Electroanalytical Chemistry, 633 (2009) 228-234.
[16] M.Ç. Canbaz, M.K. Sezgintürk, Fabrication of a highly sensitive disposable immunosensor based on indium tin oxide substrates for cancer biomarker detection, Analytical biochemistry, 446 (2014) 9-18.
[17] M. Santhosh, S.R. Chinnadayyala, N.K. Singh, P. Goswami, Human serum albumin-stabilized gold nanoclusters act as an electron transfer bridge supporting specific electrocatalysis of bilirubin useful for biosensing applications, Bioelectrochemistry, 111 (2016) 7-14.
[18] Z. Zhang, Y. Hu, H. Zhang, L. Luo, S. Yao, Layer-by-layer assembly sensitive electrochemical sensor for selectively probing l-histidine based on molecular imprinting sol–gel at functionalized indium tin oxide electrode, Biosensors and Bioelectronics, 26 (2010) 696-702.
[19] X. Li, Z. Zheng, X. Liu, S. Zhao, S. Liu, Nanostructured photoelectrochemical biosensor for highly sensitive detection of organophosphorous pesticides, Biosensors and Bioelectronics, 64 (2015) 1-5.
[20] A. Zabardasti, H. Afrouzi, R.P. Talemi, A simple and sensitive methodology for voltammetric determination of valproic acid in human blood plasma samples using 3-aminopropyletriethoxy silane coated magnetic nanoparticles modified pencil graphite electrode, Materials Science and Engineering: C, 76 (2017) 425-430.
[21] M.B. dos Santos, S. Azevedo, J. Agusil, B. Prieto-Simón, C. Sporer, E. Torrents, A. Juárez, V. Teixeira, J. Samitier, Label-free ITO-based immunosensor for the detection of very low concentrations of pathogenic bacteria, Bioelectrochemistry, 101 (2015) 146-152.
[22] S.K. Arya, A.K. Prusty, S. Singh, P.R. Solanki, M.K. Pandey, M. Datta, B.D. Malhotra, Cholesterol biosensor based on N-(2-aminoethyl)-3-aminopropyl-trimethoxysilane self-assembled monolayer, Analytical biochemistry, 363 (2007) 210-218.
[23] A.K. Yagati, T. Lee, J. Min, J.-W. Choi, Electrochemical performance of gold nanoparticle–cytochrome c hybrid interface for H 2 O 2 detection, Colloids and Surfaces B: Biointerfaces, 92 (2012) 161-167.
[24] J. Cancino-Bernardi, V.S. Marangoni, H.A. Faria, V. Zucolotto, Detection of leukemic cells by using jacalin as the biorecognition layer: A new strategy for the detection of circulating tumor cells, ChemElectroChem, 2 (2015) 963-969.
[25] A. Singh, M. Choudhary, M. Singh, H. Verma, S.P. Singh, K. Arora, DNA Functionalized direct electro-deposited gold nanoaggregates for efficient detection of Salmonella typhi, Bioelectrochemistry, 105 (2015) 7-15.

[26] A.K. Yagati, Y. Choi, J. Park, J.-W. Choi, H.-S. Jun, S. Cho, Silver nanoflower–reduced graphene oxide composite based micro-disk electrode for insulin detection in serum, Biosensors and Bioelectronics, 80 (2016) 307-314.
[27] I. Tiwari, M. Singh, C.M. Pandey, G. Sumana, Electrochemical genosensor based on graphene oxide modified iron oxide–chitosan hybrid nanocomposite for pathogen detection, Sensors and Actuators B: Chemical, 206 (2015) 276-283.
[28] C.M. Pandey, S. Dewan, S. Chawla, B.K. Yadav, G. Sumana, B.D. Malhotra, Controlled deposition of functionalized silica coated zinc oxide nano-assemblies at the air/water interface for blood cancer detection, Analytica chimica acta, 937 (2016) 29-38.
[29] G.-L. Wang, J.-X. Shu, Y.-M. Dong, X.-M. Wu, Z.-J. Li, An ultrasensitive and universal photoelectrochemical immunoassay based on enzyme mimetics enhanced signal amplification, Biosensors and Bioelectronics, 66 (2015) 283-289.
[30] Y. Zhang, B. Zhang, X. Ye, Y. Yan, L. Huang, Z. Jiang, S. Tan, X. Cai, Electrochemical immunosensor for interferon-γ based on disposable ITO detector and HRP-antibody-conjugated nano gold as signal tag, Materials Science and Engineering: C, 59 (2016) 577-584.
[31] R. Pilolli, L. Monaci, A. Visconti, Advances in biosensor development based on integrating nanotechnology and applied to food-allergen management, TrAC Trends in Analytical Chemistry, 47 (2013) 12-26.
[32] E.B. Bahadır, M.K. Sezgintürk, A comparative study of short chain and long chain mercapto acids used in biosensor fabrication: A VEGF-R1-based immunosensor as a model system, Artificial cells, nanomedicine, and biotechnology, 44 (2016) 462-470.
[33] B. Derkus, M. Ozkan, K.C. Emregul, E. Emregul, Single frequency analysis for clinical immunosensor design, RSC Advances, 6 (2016) 281-289.
[34] D. Wei, Electrochemical Nanofabrication: principles and applications, Pan Stanford2016.
[35] M.H. Jazayeri, H. Amani, A.A. Pourfatollah, H. Pazoki-Toroudi, B. Sedighimoghaddam, Various methods of gold nanoparticles (GNPs) conjugation to antibodies, Sensing and Bio-Sensing Research, 9 (2016) 17-22.
[36] R. Burry, Immunocytochemistry. A Practical Guide for Biomedical Research. 2010, Springer, Heidelberg, Germany.
[37] K. Khaldi, S. Sam, A. Gouget-Laemmel, C. Henry de Villeneuve, A. Moraillon, F. Ozanam, J. Yang, A. Kermad, N. Ghellai, N. Gabouze, Active Acetylcholinesterase Immobilization on a Functionalized Silicon Surface, Langmuir, 31 (2015) 8421-8428.
[38] J. Kong, S. Yu, Fourier transform infrared spectroscopic analysis of protein secondary structures, Acta biochimica et biophysica Sinica, 39 (2007) 549-559.
[39] N. Prabhakar, Z. Matharu, B. Malhotra, Polyaniline Langmuir–Blodgett film based aptasensor for ochratoxin A detection, Biosensors and Bioelectronics, 26 (2011) 4006-4011.
[40] M.K. Sezgintürk, A new impedimetric biosensor utilizing vegf receptor-1 (flt-1): Early diagnosis of vascular endothelial growth factor in breast cancer, Biosensors and Bioelectronics, 26 (2011) 4032-4039.
[41] P. Sobrova, M. Ryvolova, J. Hubalek, V. Adam, R. Kizek, Voltammetry as a tool for characterization of CdTe quantum dots, International journal of molecular sciences, 14 (2013) 13497-13510.
[42] B. Özcan, M.K. Sezgintürk, Graphene oxide based electrochemical label free immunosensor for rapid and highly sensitive determination of tumor marker HSP70, Talanta, 160 (2016) 367-374.
[43] B. Özcan, B. Demirbakan, G. Yeşiller, M.K. Sezgintürk, Introducing a new method for evaluation of the interaction between an antigen and an antibody: Single frequency impedance analysis for biosensing systems, Talanta, 125 (2014) 7-13.
[44] Ç.S. Şimşek, M. Teke, M.K. Sezgintürk, An ITO based disposable biosensor for ultrasensitive analysis of retinol binding protein, Electroanalysis, 26 (2014) 328-339.
[45] M. Teke, Ç. Sayıklı, Ç. Canbaz, M.K. Sezgintürk, A Novel Biosensing System Using Biological Receptor for Analysis of Vascular Endothelial Growth Factor, International Journal of Peptide Research and Therapeutics, 20 (2014) 221-230.

Figure Captions

Immobilization Scheme. Schematic diagram of the fabrication of the impedimetric MAGE-1 biosensor and the detection of MAGE-1 antigen

Figure 1. FTIR spectra of the fabrication steps of the impedimetric MAGE-1 biosensor

Figure 2. Nyquist plots and cyclic voltammograms of MAGE-1 biosensor (-▼-▼-: hydroxylated ITO electrode, -♦-♦-: ITO/CTES, -●-●-: ITO/CTES/EDC-NHS, -▲-▲-: ITO/CTES/EDC-NHS/anti-MAGE-1, -■-■-: ITO/CTES/EDC-NHS/anti-MAGE-1/BSA)

Figure 3. SEM images of proposed ITO immunosensor

Figure 4. AFM images of immobilization steps of developed immunosensor

Figure 5. (A) Nyquist plots and (C) cyclic voltammograms of MAGE-1 biosensor with different concentrations of MAGE-1 antigens, (B) calibration curve of MAGE-1 biosensor

Figure 6. SFI spectra obtained from anti-MAGE-1 antibody and MAGE-1 antigen interaction

Table 1. Results of five different human serum samples by using ELISA method and proposed immunosensor

Sample	ELISA Results (ng/mL)	Found by biosensor (ng/mL)	% Relative difference	Added MAGE-1 (ng/mL)	Total found by biosensor	Recovery
1	10.53	10.66	+1.23	4.0	14.69	100.20
2	10.51	10.52	+0.10	4.0	14.56	100.28
3	10.08	10.13	+0.50	4.0	14.10	99.79
4	10.15	10.26	+1.08	4.0	14.20	99.58
5	10.35	10.40	+0.48	4.0	14.41	100.07

Biosensor surfaces Goodness of fit values	
Kramers–Kronig transforms for different layers of the biosensor	
ITO/ OH	11.22
ITO/ OH/CTES	2.605
ITO/ OH/CTES/EDC-NHS	2.798
ITO/ OH/CTES/EDC-NHS/Anti-MAGE-1	1.324
ITO/ OH/CTES/EDC-NHS/Anti-MAGE-1/BSA	3.821
ITO/ OH/CTES/Anti-MAGE-1/BSA/MAGE-1	0.62

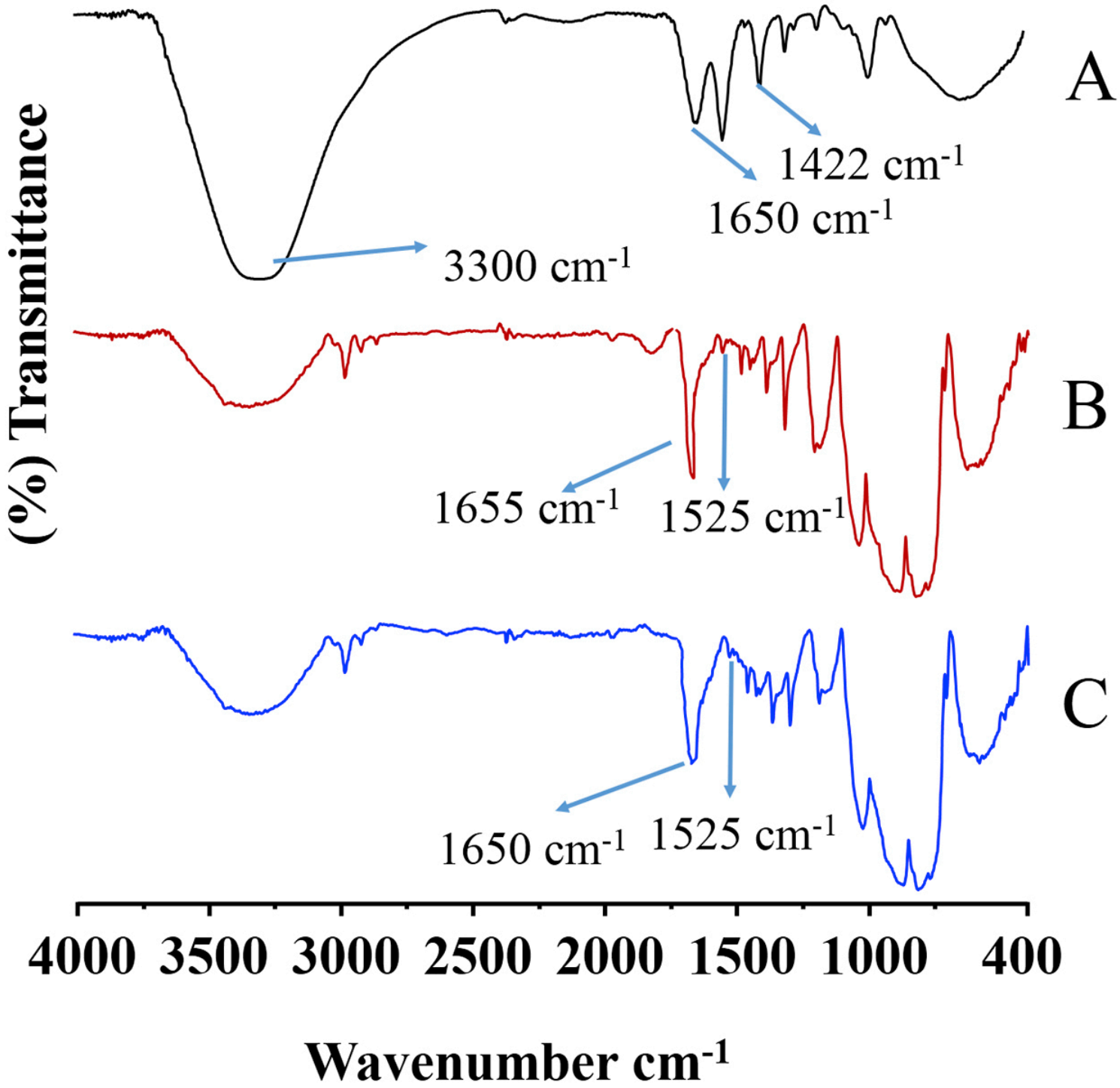
A
1422 cm-1
1650 cm-1
3300 cm-1
B
1655 cm-1
1525 cm-1
C
1650 cm-1
1525 cm-1
(%) Transmittance
4000 3500 3000 2500 2000 1500 1000 400
Wavenumber cm-1

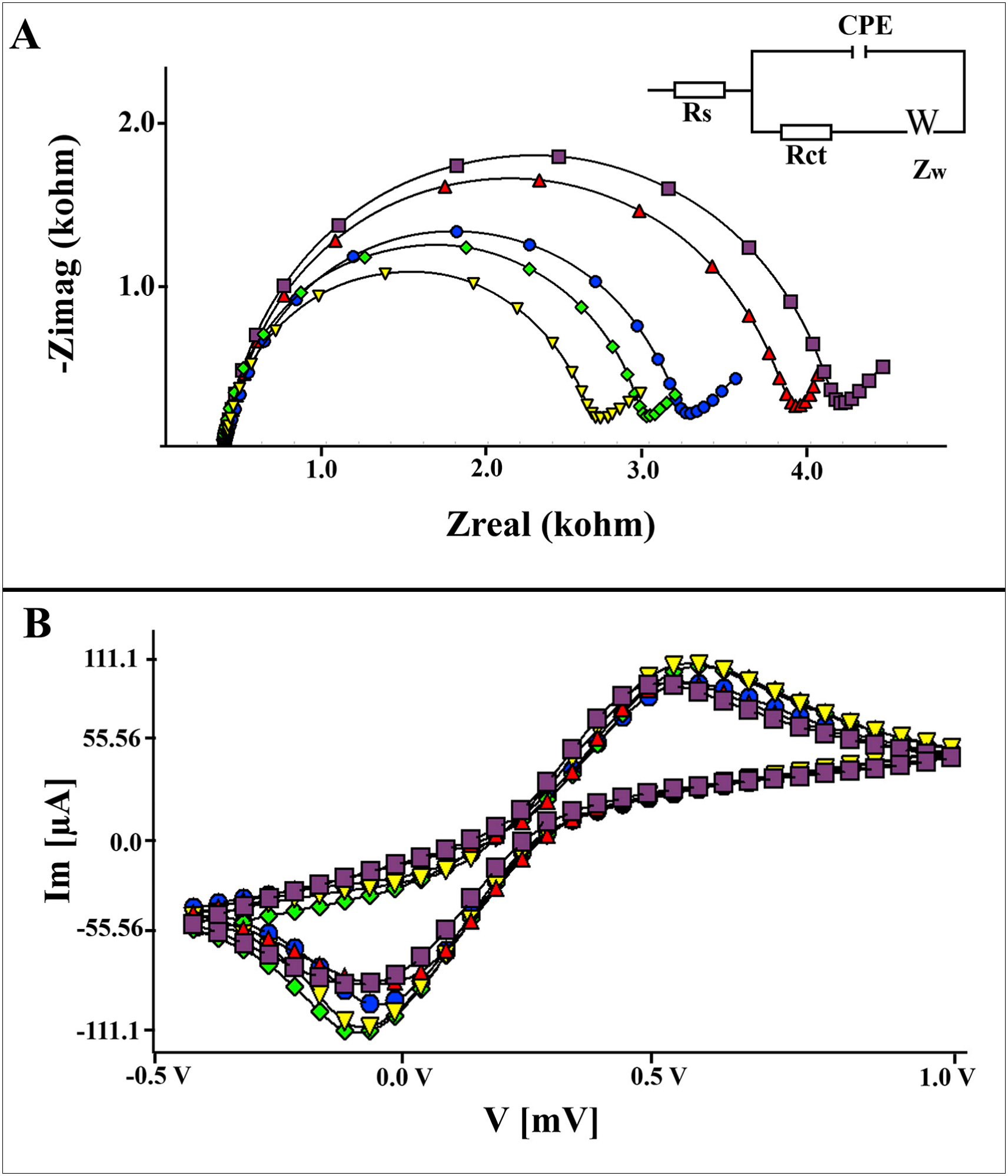
A
CPE
Rs
W
Rct
Zw
2.0
1.0
-Zimag (kohm)
1.0
2.0
3.0
4.0
Zreal (kohm)
B
111.1
55.56
0.0
-55.56
-111.1
Im [µA]
-0.5 V
0.0 V
0.5 V
1.0 V
V [mV]

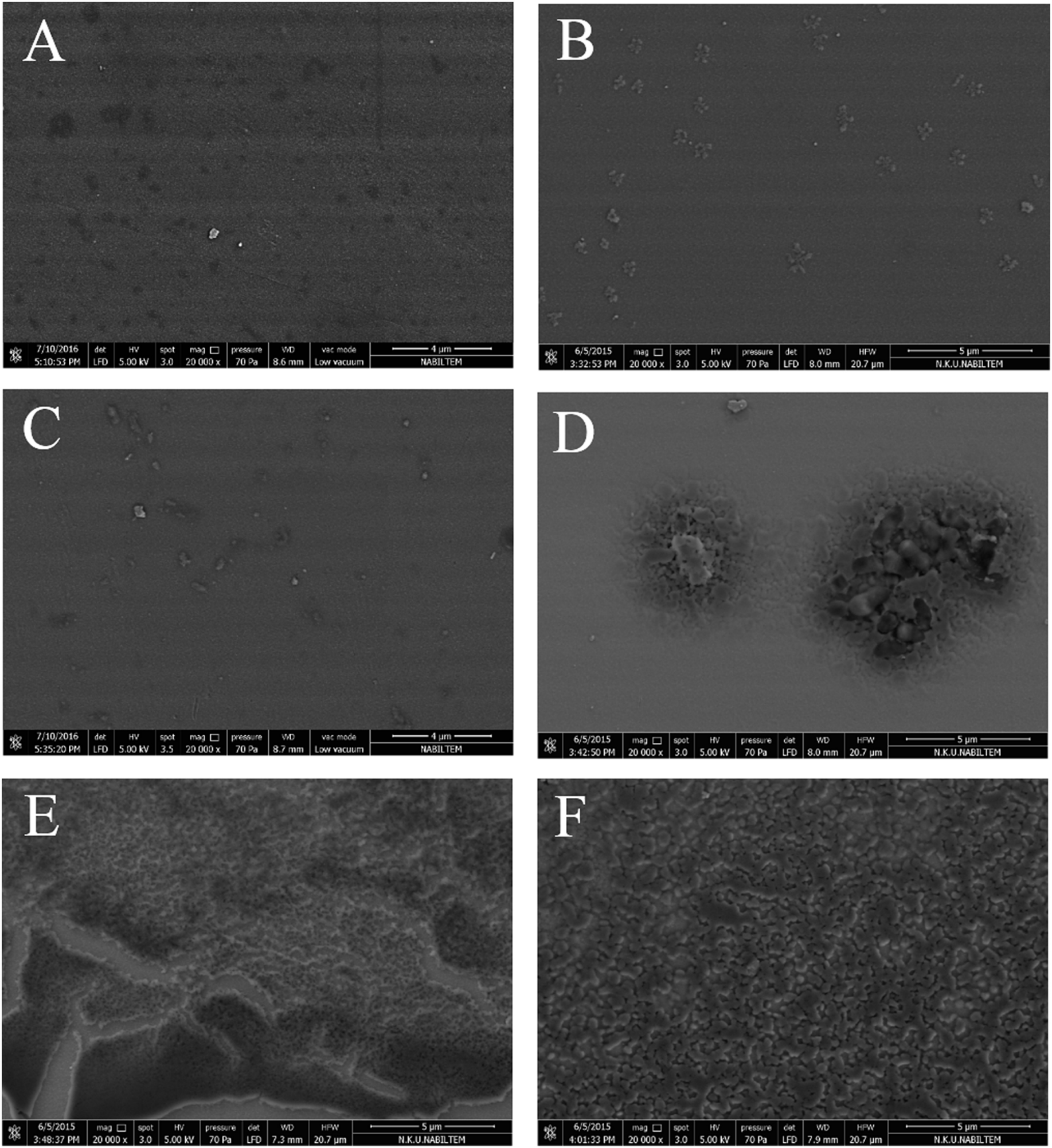
A
7/10/2016 5:10:53 PM | det LFD | HV 5.00 kV | spot 3.0 | mag 20 000 x | pressure 70 Pa | WD 8.6 mm | vac mode Low vacuum | 4 µm | NABILTEM
B
6/5/2015 3:32:53 PM | mag 20 000 x | spot 3.0 | HV 5.00 kV | pressure 70 Pa | det LFD | WD 8.0 mm | HFW 20.7 µm | 5 µm | N.K.U.NABILTEM
C
7/10/2016 5:35:20 PM | det LFD | HV 5.00 kV | spot 3.5 | mag 20 000 x | pressure 70 Pa | WD 8.7 mm | vac mode Low vacuum | 4 µm | NABILTEM
D
6/5/2015 3:42:50 PM | mag 20 000 x | spot 3.0 | HV 5.00 kV | pressure 70 Pa | det LFD | WD 8.0 mm | HFW 20.7 µm | 5 µm | N.K.U.NABILTEM
E
6/5/2015 3:48:37 PM | mag 20 000 x | spot 3.0 | HV 5.00 kV | pressure 70 Pa | det LFD | WD 7.3 mm | HFW 20.7 µm | 5 µm | N.K.U.NABILTEM
F
6/5/2015 4:01:33 PM | mag 20 000 x | spot 3.0 | HV 5.00 kV | pressure 70 Pa | det LFD | WD 7.9 mm | HFW 20.7 µm | 5 µm | N.K.U.NABILTEM

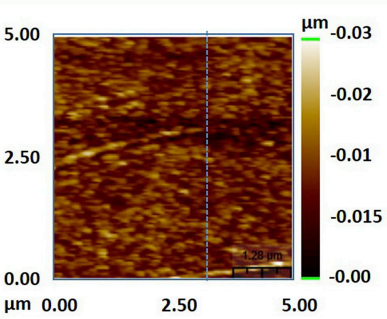

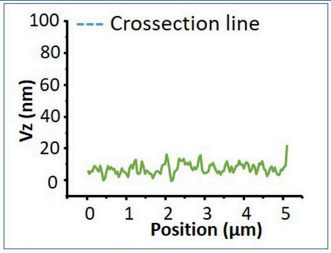

Scan Mode : Tapping AFM
Scan Size : 5.00 µm
Scan Speed : 2.5 µm/s

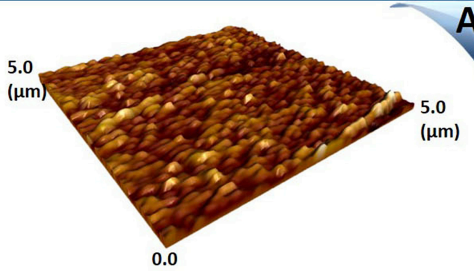

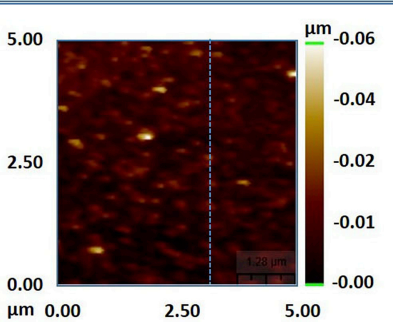

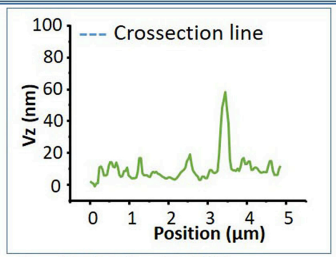

Scan Mode : Tapping AFM
Scan Size : 5.00 µm
Scan Speed : 2.5 µm/s

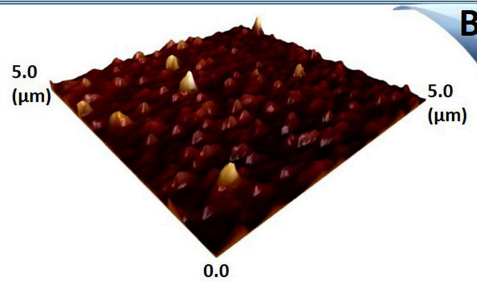

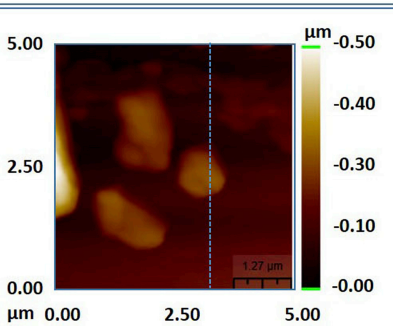

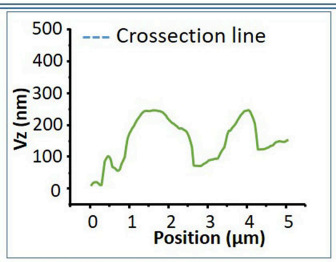

Scan Mode : Tapping AFM
Scan Size : 5.00 µm
Scan Speed : 2.5 µm/s

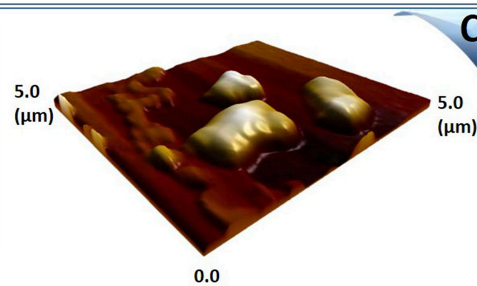

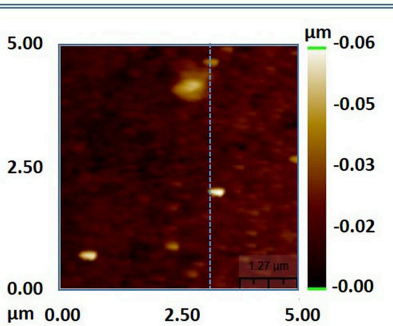

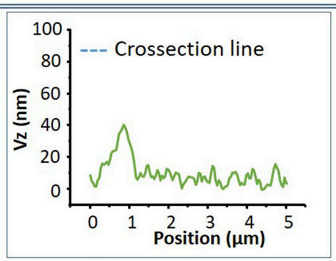

Scan Mode : Tapping AFM
Scan Size : 5.00 µm
Scan Speed : 2.5 µm/s

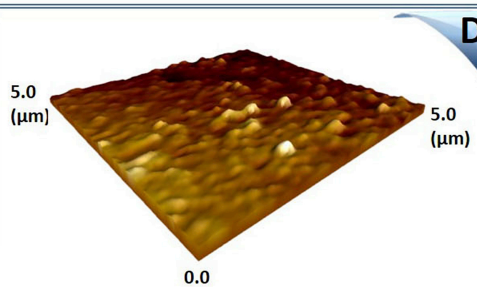

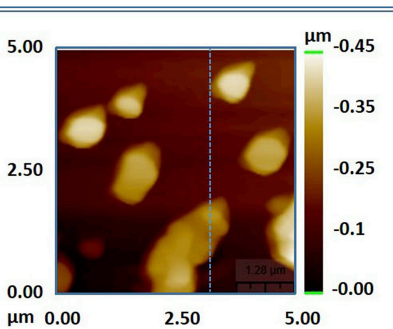

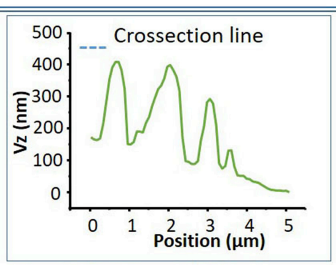

Scan Mode : Tapping AFM
Scan Size : 5.00 µm
Scan Speed : 2.5 µm/s

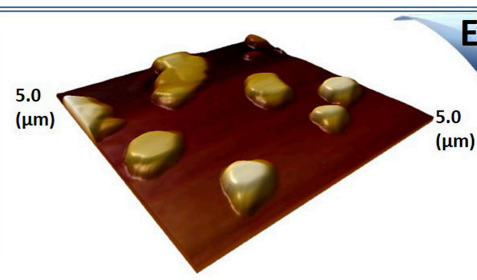

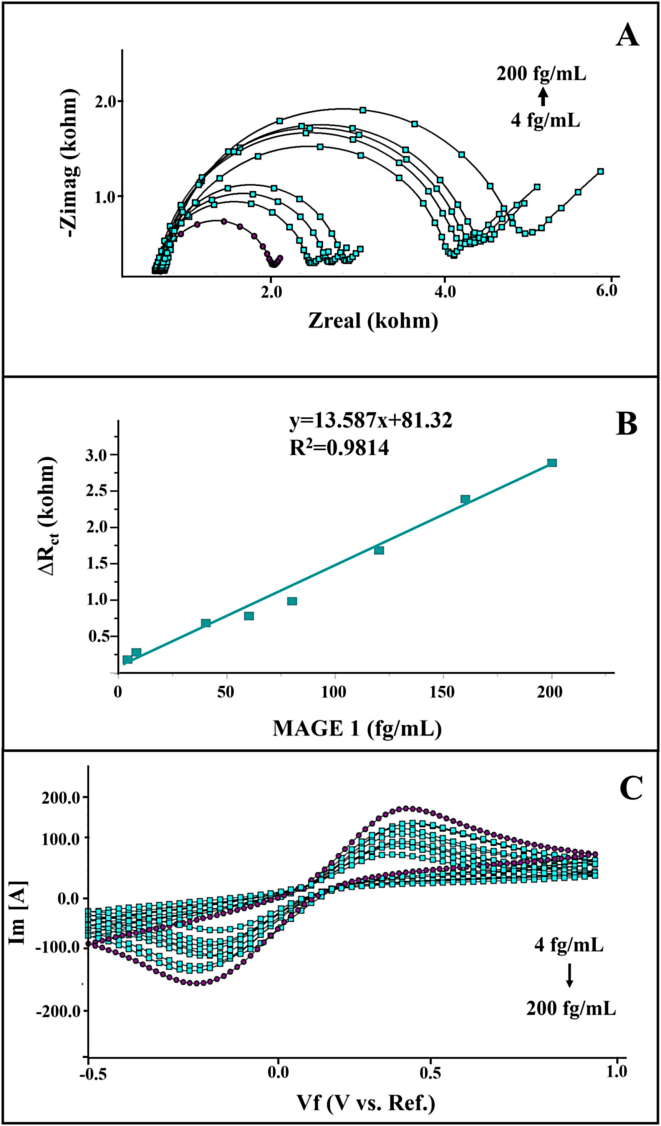
A
200 fg/mL
4 fg/mL
-Zimag (kohm)
2.0
1.0
2.0
4.0
6.0
Zreal (kohm)
B
y=13.587x+81.32
R²=0.9814
ΔRct (kohm)
3.0
2.5
2.0
1.5
1.0
0.5
0
50
100
150
200
MAGE 1 (fg/mL)
C
200.0
100.0
0.0
-100.0
-200.0
Im [A]
4 fg/mL
200 fg/mL
-0.5
0.0
0.5
1.0
Vf (V vs. Ref.)

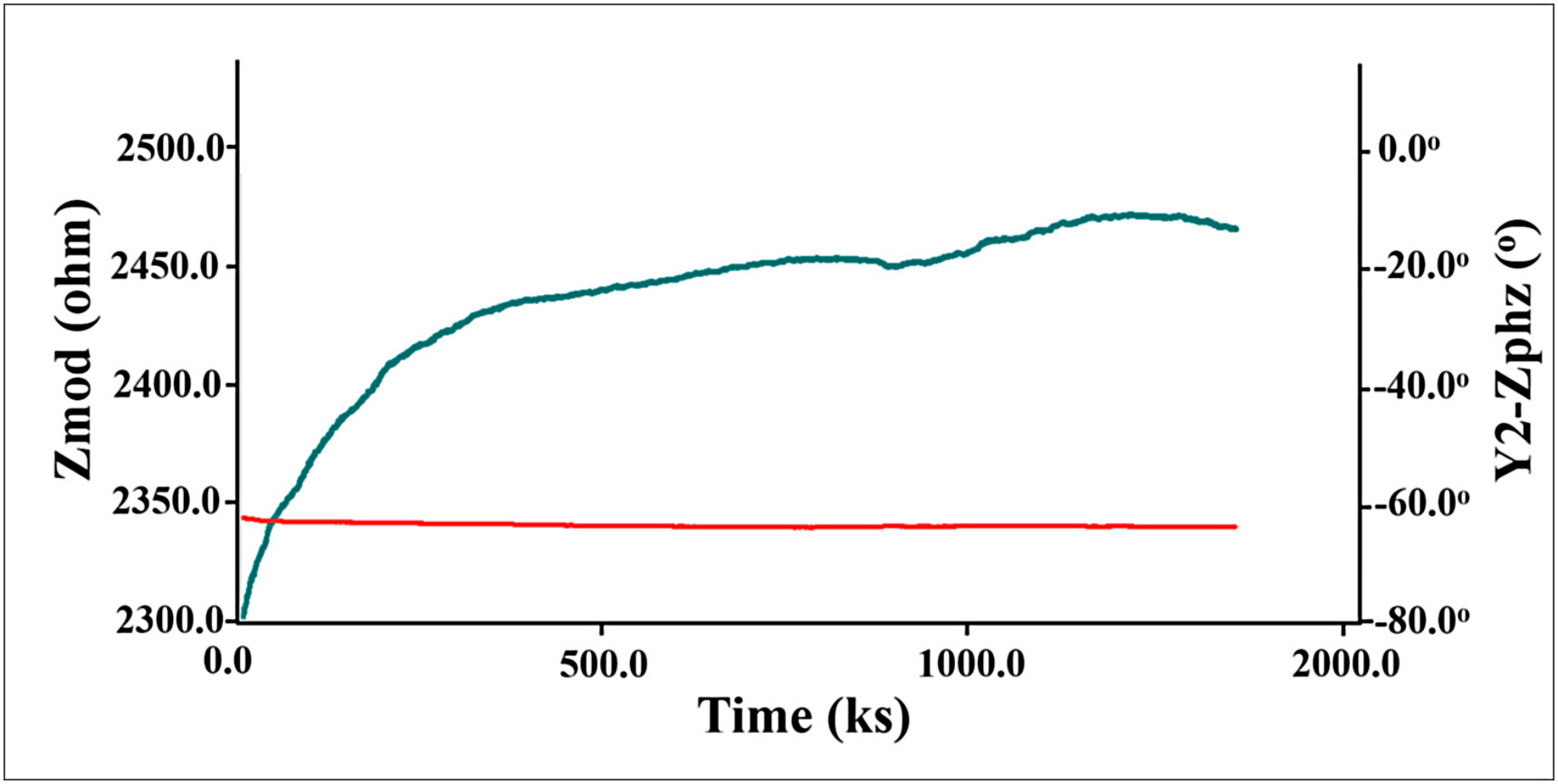
2500.0
2450.0
2400.0
2350.0
2300.0
Zmod (ohm)
0.0
500.0
1000.0
2000.0
Time (ks)
0.0°
-20.0°
-40.0°
-60.0°
-80.0°
Y2-Zphz (°)